Revised version #2

An Analysis of the Magnetic Behavior of Olivine and Garnet Substitutional Solid Solutions

Charles A. Geiger*, Michael Grodzicki and Edgar Dachs

Department Chemistry and Physics of Materials

Salzburg University

Jakob Haringer Straße 2a

A-5020 Salzburg, Austria

*corresponding author & e-mail: ca.geiger@sbg.at.ac

Tel: ++43-662-8044-6226

Fax: ++43-662-8044-622

Written on a Mac with Word Version 16.16.2

Date: 01.03.19

ABSTRACT

The low-temperature magnetic and Néel temperature, T_N, properties of four silicate substitutional solid solutions containing paramagnetic ions are analyzed. The four systems are: fayalite-forsterite olivine, $Fe^{2+}_2SiO_4$-Mg_2SiO_4, and the garnet series, grossular-andradite, $Ca_3(Al_x,Fe^{3+}_{1-x})_2Si_3O_{12}$, grossular-spessartine, $(Ca_x,Mn^{2+}_{1-x})_3Al_2Si_3O_{12}$, and almandine-spessartine, $(Fe^{2+}_x,Mn^{2+}_{1-x})_3Al_2Si_3O_{12}$. Local magnetic behavior of the transition-metal-bearing end members is taken from published neutron diffraction results and theoretical calculations. T_N values are from calorimetric heat capacity, C_p, and magnetic susceptibility measurements. These end-members, along with more transition-metal-rich solid solutions, show a paramagnetic to antiferromagnetic phase transition. It is marked by a C_p λ-anomaly that decreases in temperature and magnitude with increasing substitution of the diamagnetic component. For olivines, T_N varies between 65 K and 18 K and T_N for the various garnets is less than 12 K. Local magnetic behavior can involve one or more superexchange interactions mediated through oxygen atoms. T_N behavior shows a quasi-plateau-like effect for the systems fayalite-forsterite, grossular-andradite and grossular-spessartine. More transition-metal-rich crystals show a stronger T_N dependence compared to transition-metal-poor ones. The latter may possibly show superparamagnetic behavior. $(Fe^{2+}_x,Mn^{2+}_{1-x})_3Al_2Si_3O_{12}$ garnets show fundamentally different magnetic behavior. End-member almandine and spessartine have different and complex interacting local superexchange mechanisms and intermediate compositions show a double-exchange magnetic mechanism. For the latter, T_N values show negative deviations from linear interpolated T_N values between the end members. Double exchange occurs seldomly in oxides, and this may be the first documentation of this magnetic mechanism in a silicate. T_N behavior may possibly be used to better understand the nature of macroscopic thermodynamic functions, C_p and $S°$, of both end-member and substitutional solid solutions phases.

Keywords: Olivine, garnet, heat capacity, Néel temperature, calorimetry, solid solutions, transition metals, superexchange, superparamagnetism, double exchange, thermodynamics.

INTRODUCTION

The majority of rock-forming minerals contains transition metals. Iron, either $Fe^{2+/3+}$, is the most abundant element in terms of concentration, but Ni^{2+}, $Mn^{2+/3+}$, Cr^{3+}, and Ti^{4+} can also be considered major elements in some cases. Transition metals, even in small concentration, can play a key role in determining optical, magnetic and various transport properties in crystals. Thermodynamic behavior can also be affected by them. Their presence affects large-scale Earth processes as in redox reactions and deep mantle melting, for example. The property of paleomagnetism is based on the ability of a mineral to retain a memory of Earth's paleogeomagnetic field during crystallization.

At the simplest level, magnetism in minerals results from partially occupied *d*-shells of transition-metal ions (minerals with *f* electrons can also be magnetic, but for rock-forming minerals these electrons are less important in terms of magnetic behavior). The resulting physical property is a magnetic dipole moment generated by the spin of the electrons. In terms of classical physics, the spin can be described by an electron spinning in either a clockwise or anticlockwise (or spin up and spin down) manner. In quantum terms, this is given by the spin quantum number, where $M_S = +1/2$ or $M_S = -1/2$. Magnetic behavior in crystals is determined by the type and strength of the various interactions between the electron spins. These interactions can be of the simple dipole type or more complex ones involving additional intervening atoms (Goodenough 1963; Blundell 2001). All spin interactions are a function of temperature.

Detailed study of the magnetic behavior of crystals in the mineralogical sciences is relatively young (see Parks and Akhtar 1968, for an early work and references therein) and not extensive. In contrast, in physics and material sciences the amount of research made on the magnetic behavior of crystals is enormous. In the late 1940s important theoretical concepts were developed, synthesis experiments on various composition spinel(ferrite)- and garnet-structure crystals were started and investigations on their magnetic properties were made (e.g., Néel 1948; Winkler 1981). Many of these phases contain rare earth elements with partially occupied *f*-orbitals, but $Fe^{2+,3+}$ with *d*-electrons is important in many cases.

In contrast, little study has focused on the magnetic properties of rock-forming silicates and especially for substitutional solid solutions. The level of scientific understanding is minimal to nonexistent. In these systems, the electronic configuration of the transition metal(s), its/their structural location and concentration in a crystal are critical, because they together will determine the type of magnetic interaction(s). Fayalite, $Fe^{2+}_2SiO_4$, and fayalite-forsterite, $Fe^{2+}_2SiO_4$-Mg_2SiO_4, olivine substitutional solid solutions have received the most study. Fayalite shows a large and relatively high-temperature magnetic transition at about 65 K, but magnetic behavior at lower temperatures down to roughly 20 K is controversial (e.g., Santoro et al. 1966; Robie et al. 1982; Lottermoser et al. 1986; Aronson et al. 2007). With increasing forsterite component in Fe^{2+}-Mg olivine substitutional solid solutions, the magnetic transition temperature decreases (Dachs et al. 2007; Belley et al. 2009). The common end-member silicate garnets, almandine (Prandl 1971, Murad and Wagner 1987; Anovitz et al. 1993; Dachs et al. 2014b), spessartine (Prandl 1973; Dachs et al. 2009; Lau et al. 2009) and andradite (Murad 1984; Plakhty et al. 1993; Geiger et al. 2018) have received some experimental study and they undergo a very low temperature ($T < 12$ K) spin transition. The transition in both silicate structure types of end-member composition is of the paramagnetic-antiferromagnetic type marking a disordered to a long-range ordered spin state. It is defined by the Neel temperature, T_N, which in terms of experimental C_p measurements is expressed by a λ-anomaly.

We undertook an analysis of the magnetic behavior of the fayalite-forsterite and three garnet binary substitutional solid solutions, namely grossular-andradite, $Ca_3(Fe^{3+}_x,Al_{1-x},)_2Si_3O_{12}$, grossular-spessartine, $(Ca_x,Mn^{2+}_{1-x})_3Al_2Si_3O_{12}$, and almandine-spessartine, $(Fe^{2+}_x,Mn^{2+}_{1-x})_3Al_2Si_3O_{12}$. A knowledge of T_N behavior across a given binary join, as determined by low-temperature calorimetry or magnetic susceptibility measurements, together with an understanding of the local magnetic behavior of the one or two paramagnetic end-members, as determined via neutron diffraction and/or calculations, allows the magnetic behavior as a function of composition to be analyzed. This type of study has not been done before.

Furthermore, an analysis of magnetic behavior can help better understand crystal chemical and macroscopic thermodynamic behavior.

SAMPLES AND LOW-TEMPERATURE CALORIMETRY

The synthesis conditions or the natural localities for the various crystals of the four binary solid solutions, along with their chemical and physical characterization, have already been described in different publications. The four systems and cited descriptions, discussing the synthesis and characterization measurements, are: i) fayalite-forsterite, $Fe^{2+}_2SiO_4$-Mg_2SiO_4, olivine (von Seckendorff and O'Neill 1993), ii) grossular-andradite, $Ca_3(Al_x,Fe^{3+}_{1-x})_2Si_3O_{12}$ (Geiger et al. 2018; Dachs and Geiger 2019), iii) grossular-spessartine, $(Ca_x,Mn^{2+}_{1-x})_3Al_2Si_3O_{12}$ (Geiger 2000; Rodehorst et al. 2004) and iv) almandine-spessartine, $(Fe^{2+}_x,Mn^{2+}_{1-x})_3Al_2Si_3O_{12}$ (Geiger 2000, Geiger and Rossman 1994; Geiger and Feenstra 1997). The various samples are better than about 99% phase pure.

The low-temperature (i.e., 2 or 5 to 300 K) heat capacity, C_p, of the various crystals was measured previously with the Physical Properties Measurement System constructed by Quantum Design®. The calorimetric method and measurement set-up have been discussed numerous times (Dachs et al. 2009; 2012; 2014a, b; Geiger and Dachs, 2018; Geiger et al. 2018; Dachs and Geiger 2019) and will not be repeated here.

EXPERIMENTAL RESULTS

Low-temperature C_p behavior for synthetic olivines across the $Fe^{2+}_2SiO_4$-Mg_2SiO_4 binary are shown in Dachs et al. (2007). The magnetic transitions and their various T_N values are shown and given, respectively, in this work. The behavior of T_N across the $Fe^{2+}_2SiO_4$-Mg_2SiO_4 binary, as determined by the low-temperature C_p and also by magnetic susceptibility (Belly et al. 2009) measurements, is shown in Figure 1 and Figure 1a, respectively. T_N values are listed in Table 1.

The low-temperature C_p behavior for end-member andradite and solid-solution $Ca_3(Al_x,Fe^{3+}_{1-x})_2Si_3O_{12}$ garnets are shown in Geiger et al. (2018) and Dachs and Geiger (2019). The low-temperature C_p behavior for spessartine and $(Ca_x,Mn^{2+}_{1-x})Al_2Si_3O_{12}$ garnets are shown in Dachs et al. (2009) and Dachs et al. (2014a) and for almandine and $(Fe^{2+}_x,Mn^{2+}_{1-x})_3Al_2Si_3O_{12}$ garnets in Dachs et al. (2012) and Dachs et al. (2014b). The behavior of T_N for all three garnet binaries is displayed in Figure 2. T_N values are listed in Table 1.

Analyses of the C_p results in terms of modeling the magnetic transitions and the determination of T_N are discussed at length in the cited investigations. T_N is given by the peak temperature of the magnetic λ-anomaly.

DISCUSSION

Heat-capacity measurements and brief theory on magnetism

Thermophysical properties of crystals, including magnetic behavior, can change greatly in the vicinity of the critical temperature of a transition. The subject is broad and complex and cannot be treated here (see Gopal 1966; Grimvall 1986). Suffice it to note that heat-capacity measurements, where $C_p = (dH/dT)_P$ and H is the enthalpy, afford an excellent means of studying T_N and magnetic behavior of crystals (e.g., Stout 1961; Gopal 1966). In the case of most silicates studied to date, magnetic transitions occur below 65 K (i.e., fayalite) and usually at much lower temperatures. Thus, the magnetic interactions are weak, but in some cases they can give rise to larger $C_p(T)$ values than those deriving from atomic vibrations (phonons) at low temperatures. When it is possible to separate the vibrational (phonon or lattice) heat capacity, C_{vib}, from the magnetic heat capacity, C_{mag}, from experimental C_p measurements important information is obtained (e.g., Gopal 1966).

Experimental investigations of different types made on transition-metal-bearing olivines and garnets demonstrate that these two structure types undergo one or two magnetic or magnetic-related transitions at low temperatures. In terms of calorimetry, it is marked by a λ-

159 peak or -anomaly (i.e., 2nd order phase transition) that describes the thermophysical changes
160 resulting from the magnetic interactions, whereby disordered electron spins begin to interact
161 locally and order with decreasing temperature. The start of spin ordering (short range) coincides
162 with the onset of the high-temperature flank of the λ-peak until reaching a completely long-
163 range ordered state at the critical temperature, that is T_N.

164 According to the Heisenberg model for interacting localized spins, the effective magnetic
165 coupling constant, J_{eff}, is related to T_N (by the relationship:

166 $$J_{eff}/_k = \frac{3T_N}{zS(S+1)} \quad (1),$$

167 where k is Boltzmann's constant, S is the total spin and z is the number of nearest neighbor
168 magnetic ions [z = 2 (M1) and 4 (M2) for olivine and z = 4 (dodecahedral site) or 6 (octahedral
169 site) for garnet]. On the basis of accurate crystal-structure results, the magnetic coupling
170 constant, J, for two weakly coupled localized spins S^A and S^B can be obtained from the energy
171 difference between parallel (S_{max}) and antiparallel (S_{min}) alignment of the spins (Zherebetskyy et
172 al. 2012 and references therein). It is given by:

173 $$J = -\frac{E(S_{max}) - E(S_{min})}{S_{max}^2 - S_{min}^2} \quad (2),$$

174 where the numerically calculated $E(S)$ is the total energy for the spin state, S. Positive values of
175 J correspond to parallel or ferromagnetic and negative values to antiparallel or antiferromagnetic
176 coupling of the two spins S^A and S^B.

177

178 **Olivine and garnet crystal structures**

179 *Olivine*

180 Olivine, X_2SiO_4, with X = Fe^{2+}(fayalite) and/or Mg (forsterite), is crystallograpically
181 orthorhombic with space group *Pbnm,* and it has 4 formula units per unit cell. The crystal
182 structure is shown in Figure 3. The two crystallographically independent cations sites, excluding
183 Si, are termed *M*1 and *M*2. *M*2, Si, O1 and O2 atoms are located on mirror planes and have *m*

point symmetry. The *M*1 cation is located at the origin of the unit cell and has *-1* point symmetry, while O3 and O4 occupy general positions of symmetry *1*. A number of structural and crystal-chemical studies investigated the nature of the long-range Mg-Fe^{2+} distribution over the two *M*1 and *M*2 octahedral sites in $Fe^{2+}_2SiO_4$-Mg_2SiO_4 solid solutions. There are contradictory results and interpretations obtained over the years. The careful, recent X-ray diffraction investigation of Heinemann et al. (2007) summarize the situation on order-disorder.

Garnet

The garnet crystal structure I*a*-3*d*, general formula $\{X_3\}[Y_2](Z_3)O_{12}$, contains three different and independent cation sites (Menzer 1928; Novak and Gibbs 1971) forming a quasi-framework consisting of rigid corner-sharing ZO_4 tetrahedra and YO_6 octahedra (Armbruster et al., 1992). The structure is shown in Figure 4a. The *Y*-cations are located at the Wyckoff site 16*d* of point symmetry *-3*. The *X*-cations, located at 24*c* of point symmetry 222, are coordinated by 8 oxygen atoms in the form of a triangular dodecahedron. All sites allow for the incorporation of various cations with or without unpaired *d*- or *f*-electrons (Winkler, 1981), whereby the major cations for the common silicate garnets (*Z* = Si of point symmetry -4) are *X* = Ca, Mg, Fe^{2+} and Mn^{2+} and *Y* = Al, Fe^{3+} and Cr^{3+}. Accordingly, magnetic interactions can occur on two different sublattices that can, furthermore, interact between each other leading to varying magnetic behavior depending on the garnet chemistry. The occurrence of solid solutions, which can be extensive, of varying compositions can lead to significant changes in the physical properties of garnet (Geiger 2013).

Magnetic and T_N behavior in olivine and garnet solid solutions: Binary systems with a paramagnetic and diamagnetic end member

$Fe^{2+}_2SiO_4$-Mg_2SiO_4 olivines

Paramagnetic fayalite shows a magnetic transition at 65 K as measured experimentally several times (e.g., Santoro et al. 1966; Lottermoser et al. 1986; Robie et al. 1982; Aronson et al. 2007). Müller et al. (1982) investigated the magnetic structure of synthetic fayalite using unpolarized neutron diffraction data recorded at 4.2, 35, and 120 K. The various results show that the electronic and magnetic properties deriving from the two crystallographically independent Fe^{2+} atoms at M1 and M2 are complex. Magnetic interactions occur on the two different sublattices that interact, furthermore, between each other. The ab-initio calculations of Cococcioni et al. (2003) for the ground state of fayalite were interpreted as showing that ferromagnetic spin ordering occurs between edge-sharing octahedra (Fig. 3b, d) and antiferromagnetic ordering occurs between corner-sharing octahedra (Fig. 3c) and both through oxygen-mediated superexchange.

Forsterite is diamagnetic, but all studied forsterite-containing $Fe^{2+}_2SiO_4$-Mg_2SiO_4 solid solutions show a "λ-anomaly". T_N decreases with increasing forsterite component in the olivine as observed via calorimetry (Dachs et al. 2007) and magnetic susceptibility measurements (Belley et al. 2009). This behavior is shown in Figure 1 and supplementary Figure 1a (see data in Table 1). The intensity of the C_p λ-peak also decreases accordingly. T_N values obtained via magnetic susceptibility measurements on fayalite-rich olivines are in good agreement with those obtained from calorimetry. There are greater differences for $Fa_{50}Fo_{50}$ and $Fa_{40}Fo_{60}$ compositions. Belley et al. (2009) did not observe a transition in more forsterite-rich olivines. (Note: The errors in T_N are considered to be larger than those in Dachs et al. (2007) - Table 1). In terms of calorimetric determinations, T_N is 65 K for fayalite and T_N decreases to 18.6 K for composition $Fa_{10}Fo_{90}$.

T_N behavior across the binary join can be described using two linear segments with a break around composition $Fa_{50}Fo_{50}$. One segment is given by the T_N values from Fa_{100} to about $Fa_{50}Fo_{50}$, while the other segment describes T_N values from about $Fa_{50}Fo_{50}$ to $Fa_{10}Fo_{90}$. For the

latter, the change in T_N is less compositionally dependent. All the T_N data across the binary can also be fit by a third-order polynomial (Fig. 1).

$Ca_3(Al_x,Fe^{3+}_{1-x})_2Si_3O_{12}$ garnets

Paramagnetic andradite contains one transition-metal cation per formula unit, namely Fe^{3+}, and it is located at the 16*a* octahedral site (Fig. 4a, b and c). Plakhty et al. (1993) analyzed the nature of the magnon and magnetic exchange interactions in a natural nearly end-member andradite containing a small amount of Mn^{2+} and Al^{3+}, as well as in isostructural synthetic $Ca_3Fe^{3+}_2Ge_3O_{12}$, from inelastic neutron scattering measurements made at 4.2 K. The strongest interactions derive from $Fe^{3+}(3d^5)$. These workers concluded that magnetic superexchange occurred through the p_σ orbitals of intermediate oxygen atoms across octahedral-dodecahedra, Fe^{3+}-O-(Ca)-O-Fe^3, bridges (Fig. 4c). Meyer et al. (2010) investigated, further, the local magnetic coupling mechanisms between Fe^{3+} atoms in And_{100} using ab-initio methods. They proposed that the low-temperature antiferromagnetic transition results from weak superexchange interactions via both Fe^{3+}-O-(Si)-O-Fe^{3+} and Fe^{3+}-O-(Ca)-O-Fe^{3+} bridges (Fig. 4b, c).

The two different local interactions may possibly be expressed in the C_p behavior of end-member andradite (Geiger et al. 2018). Here, the "λ-peak" appears to show a shoulder on its low-temperature flank (Fig. 5), which is even more pronounced in terms of entropy behavior at these low temperatures - as given by $S(T) = \int (C_P/T)\, dT$ (Geiger and Dachs 2018). The shorter superexchange bridge (i.e., Fe^{3+}-O-(Si)-O-Fe^{3+}) should be marked by the higher temperature maximum intensity of the "λ-peak" at 11.3 (± 0.2) K and the longer and weaker superexchange interaction (i.e., Fe^{3+}-O-(Ca)-O-Fe^{3+}) by the low-temperature shoulder at ~5 K. Modeling of the experimental C_p data to obtain, C_{mag}, shows that the high-temperature flank of the "λ-peak" that extends above 11 K (Fig. 5). Therefore, some degree of spin ordering is expected at these

259 temperatures. More research is needed to address the precise physical nature of the λ-peak in
260 andradite.

261 Grossular is diamagnetic, but all studied andradite-containing $Ca_3(Al_x,Fe^{3+}_{1-x})_2Si_3O_{12}$
262 solid solutions show a "λ-anomaly". T_N decreases with increasing grossular component in the
263 garnet from 11.3 K in And_{100} (Murad 1984; Geiger et al. 2018) to about 3 K for the most
264 grossular-rich garnets roughly $Gro_{80}And_{20}$ (Figure 2 with T_N values given in Table 1). The
265 intensity of the "λ-peak" also decreases with increasing grossular component in the garnet
266 (Dachs and Geiger 2019). Both indicate a weakening of the local magnetic interactions. The T_N
267 data across the join can be fit with two linear segments with a break occurring around
268 $And_{50}Gro_{50}$ (Fig. 2) or with a third-order polynomial.

269

270 *$(Ca_x,Mn^{2+}_{1-x})_3Al_2Si_3O_{12}$ garnets*

271 Paramagnetic spessartine contains one transition-metal cation per formula unit, namely
272 Mn^{2+}, that is located at the 24*c* dodecahedral site (Fig. 4a). Prandl (1973) investigated the
273 magnetic structure of synthetic spessartine using neutron powder data. Spessartine shows a λ-
274 anomaly at T_N = 6.2 K (Fig. 5 - Dachs et at. 2009) and magnetic susceptibility measurements
275 give a transition at 7 K (Lau et al. 2009). Short-range spin ordering of $Mn^{2+}(3d^5)$ begins above
276 this temperature.

277 As stated above, grossular is diamagnetic but all studied spessartine-containing
278 $(Ca_x,Mn^{2+}_{1-x})_3Al_2Si_3O_{12}$ solid solutions show a "λ-anomaly". T_N values for spessartine and
279 $(Ca_x,Mn^{2+}_{1-x})_3Al_2Si_3O_{12}$ solid-solution garnets are plotted in Figure 2 (values in Table 1).
280 Starting from Sps_{100} and moving to more grossular-rich garnets, T_N decreases from 6.2 K to
281 about 2.2 K for the $Sps_{50}Gro_{50}$ composition. At grossular-rich compositions, T_N shows a
282 plateauing behavior with T_N values ≤ 2.0 K (Table 1). A precise determination of T_N for the
283 most grossular-rich garnets is difficult due to their weak and broad λ-peaks. Moreover, our C_p

284 measurements can only be made down to 2 K. T_N behavior across the join can, once again, be
285 described using two linear segments or a third-order polynomial.
286
287 *Magnetic behavior as a function of composition*
288 All the experimental data on olivine show a decreasing and nonlinear behavior in T_N
289 across the $Fe^{2+}_2SiO_4$-Mg_2SiO_4 join. T_N, marking a paramagnetic-antiferromagnetic transition,
290 decreases from Fa_{100} to $Fa_{10}Fo_{90}$ with a quasi-plateauing behavior for forsterite-rich
291 compositions. The magnetic structure in the fayalite-rich solid solutions should be governed, as
292 in Fa_{100} (Cococcioni et al. 2003), by superexchange interactions through oxygen among Fe^{2+}
293 cations (Fig. 3b, c and d). A decrease in the intensity of the λ-peak as a function of composition
294 also demonstrates a weakening of the local magnetic interactions.
295 Analogous T_N behavior is observed for $Ca_3(Al_x,Fe^{3+}_{1-x})_2Si_3O_{12}$ and $(Ca_x,Mn^{2+}_{1-x})_3Al_2Si_3O_{12}$ garnets and the variation in magnetic properties could be similar to that in olivine.
297 Andradite and spessartine transition to an antiferromagnetic state and this is also considered the
298 case for andradite- and spessartine-rich solid solutions. For both binaries, T_N shows a quasi-
299 plateau-like effect, whereby T_N is more strongly temperature dependent in garnets richer in
300 paramagnetic cations compared to those richer in diamagnetic ones, namely Al^{3+} and Ca^{2+},
301 respectively.
302 T_N for all three solid-solution binaries appears to exhibit a change in temperature
303 dependence roughly around the 50:50 composition region. Notably, magnetic ordering persists
304 in paramagnetically-dilute solid solutions and in the case of olivine even for the Fe^{2+}-poor
305 composition $Fa_{10}Fo_{90}$. Superexchange is responsible for magnetic ordering in the transition-
306 metal-bearing end members and as well, we think, for the magnetic-cation-rich compositions.
307 However, it would appear to be difficult for superexchange to persist in compositions richer in
308 the diamagnetic component, because superexchange is a local interaction, decreasing

exponentially in strength with distance. The observed magnetic ordering in diamagnetic-component-rich solutions requires long-range interactions. What are the alternatives?

The first and most obvious one is dipolar interactions between randomly distributed isolated magnetic ions. An estimate of the order of magnitude of the magnetic energy, U_{mag}, of the dipole interaction between two free Fe^{2+} cations, for example, with (anti)parallel alignment is given by

$$U_{mag} \cdot 10^{-23}\mathrm{J} \cdot \frac{\mu^2(\mathrm{Fe}^{2+})}{x^3} \approx 1.25\ \mathrm{K} \cdot \frac{\mu^2(\mathrm{Fe}^{2+})}{x^3} \qquad (3),$$

where $\mu_B = 9.28 \cdot 10^{-24}$ A m^2 is the Bohr magneton, $\mu\,(Fe^{2+}) = 4.90$, the magnetic moment of Fe^{2+} in units of μ_B, $\mu_o = 4\pi \cdot 10^{-7}$ is the permeability of the vacuum, and x is the distance in Ångström between the dipoles. Since dipole-dipole interactions vary as $1/x^3$, they are long-range in nature. Although dipolar interactions have been shown to be significant in low-dimensional systems (Panissod and Drillon 2003), a rough estimate demonstrates that this cannot explain the observed magnetic ordering in the magnetically diluted olivine and garnet systems. For instance, in andradite with a lattice constant of 12.05 Å at 100 K (Armbruster and Geiger 1993), the assumption of randomly distributed magnetic Fe^{3+} ions in $And_{20}Gro_{80}$ yields average distances between about 7 and 10 Å. Substituting these values in eqn. (3), estimated T_N values in the range of 8 to $3 \cdot 10^{-2}$ K are obtained, i.e. about two orders smaller than the experimental ones. Similar results yield estimates of $2.75 \cdot 10^{-2}$ K for $And_{20}Gro_{80}$ using mean field theory. In the case of olivine, a value of $4 \cdot 10^{-2}$ K for $Fa_{10}Fo_{90}$ is calculated compared with the observed value of 18.6 K (calculations of R.J. Harrison, private communication). From this first-order analysis, it follows that magnetic dipole-dipole interactions cannot provide the dominating mechanism for spin ordering in diamagnetic-rich crystals.

Alternatively, magnetic ordering may occur in the form of superparamagnetism as observed, e.g., in systems of magnetic nanoparticles embedded in non-magnetic matrices (Bedanta and Kleemann 2009). This implies, as the basic assumption, that the distribution of magnetic ions in dilute solid solutions is not random but that clustering is preferred. That is, in

the more traditional sense, where nanoparticle-like magnetic aggregates are embedded in a nonmagnetic "matrix". In other words, short-range-cation order should be present in the solid solutions. This proposal may get support by the fact that cation clustering is energetically favorable, in a thermodynamic sense, due to local superexchange within a nanoparticle-like aggregate compared to a nonmagnetic one.

In summary, one possible interpretation of all the data is that two different magnetic mechanisms may be operating across the $Fe^{2+}_2SiO_4$-Mg_2SiO_4, $Ca_3(Al_x,Fe^{3+}_{1-x})_2Si_3O_{12}$ and $(Ca_x,Mn^{2+}_{1-x})_3Al_2Si_3O_{12}$ joins. In terms of olivine, Belley et al. (2009) stated that "magnetic properties do not vary linearly with iron content". It is notable that the observed T_N behavior is independent of a particular chemical composition or crystal structure. In both the olivine and the two garnet systems, roughly at the 50:50 composition, the nature of the magnetic interactions changes from local superexchange to long-range interactions possibly between magnetic nanoparticle-like aggregates. If this proposal for T_N behavior is correct, it is the first report of variable magnetic behavior for a silicate solid solution as well as magnetic cation ordering to the best of our knowledge.

Can short-range cation order occur in garnet or olivine solid solutions?

The question of short-range-cation order in silicate solid solutions has been addressed using ^{27}Al and ^{29}Si MAS NMR spectroscopy. It has been proposed to occur in diamagnetic pyrope-grossular garnets, $(Mg_x,Ca_{1-x})_3Al_2Si_3O_{12}$ (Bosenick et al. 1995; 1999; 2002). Indeed, NMR spectroscopy is the best experimental method in terms of addressing this issue, which is by no means trivial. The experimental problem becomes even more challenging in the case of systems containing paramagnetic ions. The experiments involve the measurement of para-magnetically shifted peaks, whose position is far outside the common range of non-paramagnetic chemical shifts. The resonance assignments and their analysis are not always straightforward. The results on various garnet systems appear to be the most well understood (i.e., Palke et al. 2015; Palke and Geiger 2016). Here, at this stage of research, the spectra do not

appear to show any overt or measurable short-range cation order, that is, clustering. The NMR spectra of forsterite-rich olivines are much more complex and little can be said, because the spectra show many paramagnetically shifted resonances of which nearly all cannot be assigned (McCarty et al. 2015; Stebbins 2018).

Magnetic and T_N behavior in the $(Fe^{2+}_x,Mn^{2+}_{1-x})_3Al_2Si_3O_{12}$ garnet solid solution: A binary system with two paramagnetic end-members

The third garnet binary under study has two transition metals that can occur locally at the 24*c* position (Fig. 4a and d). Low-temperature single-crystal neutron (Prandl 1971) and ^{57}Fe Mössbauer measurements (Murad and Wagner 1987) show that almandine undergoes a spin transition from a paramagnetic to an antiferromagnetic state. A λ-peak at about 9.2 K was measured via calorimetry (Anovitz et al. 1993 and Dachs et al. 2012), as shown in Figure 5. The local magnetic structure of almandine in the ground state was investigated by density functional cluster calculations (Zherebetskyy et al. 2012). The interactions causing the transition are complex. The spins of the $Fe^{2+}(3d^6)$ ions at 24*c* of the edge-shared dodecahedra sublattice (i.e., Fe^{2+}-O-Fe^{2+} - Fig. 4d) interact ferromagnetically via superexchange involving intermediate oxygen atoms. Two such separate sublattices are present and they interact further through another superexchange involving connecting SiO_4 and AlO_6 groups via Fe^{2+}-O-(Si)-O-Fe^{2+} and Fe^{2+}-O-(Al)-O-Fe^{2+} bridges. Macroscopically, the paramagnetic-antiferromagnetic transition results.

The local magnetic interactions for intermediate $(Fe^{2+}_x,Mn^{2+}_{1-x})_3Al_2Si_3O_{12}$ garnets are most interesting, because they are totally unlike the other two garnet solid solutions discussed above. $(Fe^{2+}_x,Mn^{2+}_{1-x})_3Al_2Si_3O_{12}$ garnets show nonlinear and negative T_N behavior across the binary between Sps_{100} and Alm_{100} (Fig. 2). There is no plateauing-like behave towards either end member. The high-spin *d*-electron configurations are $(d\uparrow^5 d\downarrow^1)$ for Fe^{2+} and $(d\uparrow^5)$ for Mn^{2+}. If both cations are present in a solid-solution crystal, this may lead to another type of magnetic

388 interaction known as double exchange. This mechanism was first described by Zener (1951)
389 between Mn^{3+} and Mn^{4+} in nominal $LaMnO_3$ perovskite, whereby some La^{3+} can be replaced by
390 divalent Ca, Ba or Sr, which are then charge balanced by Mn^{4+} (i.e., $La^{3+}Mn^{3+}$ = [Ca, Ba, Sr]$^{2+}$-
391 Mn^{4+}). Further analysis of the physics behind double exchange was given by Anderson and
392 Hasegawa (1955) and de Gennes (1960). The mechanism is well known in solid-state physics
393 and materials science, but it, as best we know, has never been reported in rock-forming
394 minerals. It may occur in certain garnet solid solutions having two divalent magnetic cations at
395 24*c* but with different electronic configurations. For $(Fe^{2+}_x,Mn^{2+}_{1-x})_3Al_2Si_3O_{12}$ garnets, assuming
396 parallel alignment for the total spins of both ions, $Fe^{2+}(d\uparrow^5 d\downarrow^1)$-$Mn^{2+}(d\uparrow^5)$ with $M_s(Fe^{2+}) = +2$
397 and $M_s(Mn^{2+}) = +5/2$, the single spin-down electron of Fe^{2+} can delocalize towards Mn^{2+},
398 thereby stabilizing the magnetic state. Indeed, electron delocalization leads to a decrease in
399 kinetic energy in accordance with the Heisenberg uncertainty principle. This delocalization
400 cannot occur for antiparallel alignment of spins, that is, $Fe^{2+}(d\uparrow^5 d\downarrow^1)$-$Mn^{2+}(d\downarrow^5)$ with $M_s(Fe^{2+})$ =
401 +2 and $M_s(Mn^{2+}) = -5/2$ as being inconsistent with the Pauli exclusion principle. Consequently,
402 the ferromagnetic and the stronger total antiferromagnetic interaction energy observed in Alm_{100}
403 (T_N = 9.2 K) and Sps_{100} (T_N = 6.2 K) is weakened in the solid solution. Thus, T_N shows negative
404 deviations from linearity between both end-member garnets for intermediate compositions (Fig.
405 2).

406 If magnetic double exchange does occur in $(Fe^{2+}_x,Mn^{2+}_{1-x})_3Al_2Si_3O_{12}$ garnets, not only is
407 the magnetic energy lowered, but also the total energy of the system, albeit very slightly. It
408 follows that there must be a thermodynamic driving force, again very slight, that maximizes the
409 number of local Fe^{2+}_x-Mn^{2+}_{1-x} groupings (i.e., anticlustering). In other words, there would be
410 unfavorable energetics against forming almandine- or spessartine-like clusters.
411
412 **Effect of "impurity" atoms on T_N**

Some of the minor scatter in T_N values for almandine-spessartine garnets (Geiger and Rossman 1994; Geiger and Feenstra 1997), or any garnet for that matter, may result from small amounts of "extra" cations that are not included in the ideal crystal-chemical formulae. Early indications of this are observable in the ^{57}Fe Mössbauer spectra of almandine (Murad and Wagner 1987) and inelastic neutron scattering results on andradite (Plakhty et al. 1993). T_N of synthetic almandine can be shifted to slightly lower temperatures by the presence of small amounts of octahedral Fe^{3+} (Dachs et al. 2012). The measurable effect of " extra impurity" atoms in small concentrations on T_N in garnet is apparently confirmed.

This is of note because small concentrations of octahedral Fe^{3+} occur in many synthetic and natural almandine crystals (Murad and Wagner, 1987; Geiger et al. 1988; Quartieri et al. 1993; Woodland et al. 1995). Furthermore, at high pressure there is complete solid solution between almandine and skiagite, ideally $Fe^{2+}_3Fe^{3+}_2Si_3O_{12}$ (Woodland and O'Neill 1993), and, here, the magnetic interactions can be expected to be highly complex.

Magnetic interactions and transitions: Their effect on macroscopic thermodynamic properties and the role of crystal chemistry

Compositionally end-member silicates

Both olivines and garnets are orthosilicates, but they are fundamentally different in terms of crystal structure. Fayalite has considerably stronger magnetic interactions than garnet, by nearly an order of magnitude. Indeed, the magnons associated with the magnetic phase transition in end-member fayalite at 65 K contribute more to $C_p(T)$ than phonons between 0 K and about 70 K (Dachs et al. 2007). The relatively energetic magnons derive from the closed-packed olivine structure in which the Fe^{2+} cations are relatively close to each other in M1 and M2 polyhedra and the cations can interact magnetically in several ways (Fig. 3). The two coordination octahedra have shared edges and corners. In fayalite, magnons contribute significantly to the macroscopic thermodynamic behavior at standard conditions. The standard third-law entropy, $S°$, of a crystal is given by:

$$S° - S^{T=0K} = \int_0^{298.15\,K} \frac{C_P}{T}\,dT \quad (4),$$

assuming $S^{T=0K} = 0$. For fayalite S_{mag}(298.15 K) is 26.2 J/(mol·K) and it contributes about 17% to $S°$ that is equal to 151.4 J/(mol·K) - (Dachs et al. 2007).

In the case of end-member garnet with transition-metal cations just occurring at the octahedral site, superexchange interactions are mediated through diamagnetic SiO_4 and/or XO_8 groups (Fig. 4). Thus, the interactions are very weak and magnons occur at very low energies. Andradite is a case in point. The modelled S_{mag}(298.15 K) is 28.1 J/(mol·K) and it contributes about 9% to $S°$ that is 325.0 J/(mol·K) - (Geiger and Dachs, 2018). For garnets with transition-metal cations just at the dodecahedral site, the magnetic interactions appear to be even more subtle and complex. The total magnetic interactions involve diamagnetic SiO_4 and AlO_6 groups and they do not occur directly between edge-shared dodecahedra (Zhrebetskyy et al. 2012), as might be expected from a first-order crystal-chemical analysis. Thus, the corresponding magnon energies are also weaker than in fayalite. For almandine the modelled S_{mag}(298.15 K) is 32.1 J/(mol·K) and it contributes roughly 10% to $S°$, that is 336.7 J/(mol·K) - (Dachs et al. 2012). For spessartine the model S_{mag}(298.15 K) is about 38 J/(mol·K) and $S°$ is 335.3 J/(mol·K) - (Dachs et al. 2009), thus making up about 11% of the latter. The relevant equation giving the theoretical S_{mag} value is:

$$S_{mag} = R\ln(2S + 1) \text{ per mole of cation } = 29.79 \text{ J/mol·K} \quad (5),$$

where R is the gas constant and $(2S + 1)$ is the multiplicity, i.e, the number of electron spin orientations. Only for andradite and fayalite is the agreement between model and theoretical S_{mag} values reasonable or good.

What can be stated, further, in terms of magnetic and $C_p(T)$ and S(T) behavior? Various purely empirical C_p models, such as corresponding states models (Anovitz et al. 1993; Lau et al. 2009), or more "seemingly" rigorous lattice-dynamic-type calculations (Gramaccioli et al. 2003; Gramaccioli and Pilati, 2003; Pilati et al. 1996) including neutron scattering measurements (Mittal et al. 2000) have been undertaken on garnet. Their soundness, especially,

in the former cases is questionable. We have been using the simplified lattice dynamic formulation of Komada (1986) and Komada and Westrum (1997) to model $C_{p,\mathrm{vib}}(T)$ and $S_{\mathrm{vib}}(T)$ behavior, where "vib" stands for vibrational, using experimental calorimetric $C_p^{cal}(T)$ results as input data. If the two former functions can be modeled properly, $C_{p,\mathrm{mag}}(T)$ and $S_{\mathrm{mag}}(T)$ contributions can be obtained from the difference in values (e.g., $C_{p,\mathrm{mag}}(T) = (C_p^{cal}(T) - C_{p,\mathrm{vib}}(T))$ - see Dachs et al. 2009, 2012; 2014a, b; Geiger et al. 2018, for more detail). An assumption of this model is that there are no or very minor phonon-magnon interactions. It turns out in some cases (i.e., almandine, and spessartine) that the model $S_{\mathrm{mag}}(298.15\ \mathrm{K})$ values are less than those obtained via (5). One possibility that could explain the discrepancy is that phonon-magnon coupling is occurring. Research in this direction is needed.

Substitutional solid solution silicates

The results of this investigation may help in yet another area involving thermodynamic properties. It involves macroscopic thermodynamic mixing behavior, namely $\Delta C_p^{\mathrm{mix}}(T)$ and $\Delta S^{\mathrm{mix}}(T)$, for solid solutions containing a transition metal ion or ions (see Dachs et al. 2007, 2014a, b; Dachs and Geiger 2019). In short, a precise determination of $\Delta C^{\mathrm{mix}}{}_{\mathrm{mag}}(T)$ and $\Delta S^{\mathrm{mix}}{}_{\mathrm{mag}}(T)$ behavior, obtained from an application of the Komada and Westrum (1997) model, can be problematic if they are small in magnitude. However, T_N behavior for a solid solution can help qualitatively in this question, because it can be measured precisely and it is not in any respect model dependent. Consider the system olivine (Figure 1). Dachs et al. (2007) argued that $\Delta S^{\mathrm{mix}}{}_{\mathrm{mag}}(298.15\ \mathrm{K})$ behavior shows slight negative deviations from ideality across the $Fe^{2+}{}_2SiO_4$-Mg_2SiO_4 join (i.e., $\Delta S^{\mathrm{mix}}{}_{\mathrm{mag}} < 0$). T_N behavior shows as well negative deviations from linearity (Fig 1) between Fa_{100} and $Fa_{10}Fo_{90}$. It must be noted, on the other hand, that a similar relationship does not appear to exist for andradite-grossular or spessartine-garnet garnets, where in both cases $\Delta S^{\mathrm{mix}}{}_{\mathrm{mag}}(298.15\ \mathrm{K}) = 0$.

This is a preprint, the final version is subject to change, of the American Mineralogist (MSA)
Cite as Authors (Year) Title. American Mineralogist, in press.
DOI: https://doi.org/10.2138/am-2019-6839CCBYNCND

IMPLICATIONS AND CONCLUSIONS

An understanding of the magnetic behavior of silicates, and especially their solid solutions, in both a solid-state physical and mineralogical context, is in its infancy. Little is known and much research remains to be done. In addition to the results presented above, several notable implications can be drawn from this first investigation on olivine and garnet.

First, we conclude based on our analysis, herein, that the observed λ-anomaly in the low-temperature $C_p(T)$ results on synthetic uvarovite, $Ca_3Cr^{3+}_2Si_3O_{12}$, and knorringite, $Mg_3Cr^{3+}_2Si_3O_{12}$ (Klemme et al., 2005; Wijbrans et al., 2014) is caused by a paramagnetic-antiferromagnetic transition. It must be expected that most, if not all, transition-metal-bearing silicate and germanium garnets will have very low-temperature magnetic spin transitions. This may be true for other silicates as well. A determination of their heat-capacity and magnetic behavior will require measurements down to the lowest possible temperatures. This was not always done in the past and it led to incorrect results (see the case for andradite - Geiger et al. 2018).

Second, other silicate-solid-solution systems with a paramagnetic and diamagnetic end member need to be investigated. It has to be determined, for example, how T_N behaves as a function of composition. The systematics need to be more fully studied so that a deeper scientific understanding can be reached.

Third, it can be proposed that double exchange interactions may occur among other magnetic ions than just between Fe^{2+} and Mn^{2+}. In terms of garnet, it may occur, for example, between Fe^{2+} at 24*c* and Fe^{3+} at 16*a* in certain garnets. For example, double exchange may possibly occur in certain andradites and almandines, where C_p results show small variations in T_N and λ-anomaly behavior among different crystals (Geiger et al. 2018; Dachs et al. 2012). Furthermore, several rock-forming silicate systems show an exchange between Fe^{2+} and Mn^{2+} and, here, magnetic double exchange may occur. This goes, for example, for the fayalite-tephroite (Mn_2SiO_4) join (Burns and Huggins, 1972). Marked exchange of Mn^{2+}-Fe^{2+}-(Mg)

518 cations occurs in pyroxenes, amphiboles and micas. In all these silicates, Mn^{2+} and Fe^{2+} can be
519 found in corner- and edge-shared octahedral sites and, thus, d-electron delocalization could be
520 expected.

521 Finally, and almost needless to say, the precise magnetic behavior of many solid-solution
522 silicates, containing two or more different transition-metal cations, may prove to be complex in
523 nature. Their low-temperature C_p and magnetic behavior can be expected to be complicated by
524 virtue of the range of possible chemistries and structural sites. The number of different local-
525 electron-spin interactions is expected to be large.

526

527 **ACKNOWLEDGEMENTS**

528 E.C. Ferré (Lafayette, Louisiana) kindly supplied the data from the magnetic susceptibility
529 measurements on olivine. This study was supported by a grant to C.A.G. from the Austrian
530 Science Fund (FWF: P 30977-NBL). We thank the two referees, and especially R.J. Harrison
531 (Cambridge, UK), whose keen review encouraged us to consider more fully the possible role of
532 superparamagnetism instead of dipole-dipole interactions in the solid solutions. The editor S.
533 Speziale (Potsdam, Germany) also provided useful remarks on improving the clarity of the
534 manuscript.

References Cited

Anderson, P.W. and Hasegawa, H. (1955) Considerations on double exchange. Physical Review. 100, 675-681.

Anovitz, L.M., Essene, E.J., Metz, G.W., Bohlen, S.R., Westrum Jr. E.F., and Hemingway B.S. (1993) Heat capacity and phase equilibria of almandine, $Fe_3Al_2Si_3O_{12}$. Geochimica et Cosmochimica Acta. 57, 4191-4204.

Armbruster, T., Geiger, C.A., and Lager, G.A. (1992) Single crystal X-ray refinement of almandine-pyrope garnets at 298 and 100 K. American Mineralogist. 77, 512-523.

Aronson, M.C., Stixrude, L., Davis M.K., Gannon, W., and Ahilan, K. (2007) Magnetic excitations and heat capacity of fayalite, Fe_2SiO_4. American Mineralogist. 92, 481-490.

Belley, F., Ferré, E.C., Fátima, M-H., Jackson, M.J., Dyar, M.D., and Catlos, E.J. (2009) The magnetic properties of natural and synthetic $(Fe_X,Mg_{1-X})_2SiO_4$ olivines. Earth and Planetary Sciences Letters. 284, 516-526.

Bedanta, S. and Kleemann, W. (2009) Supermagnetism. Journal of Physics D. Applied Physics. 42, 1-28.

Blundell, S. (2001) Magnetism in condensed matter. 238 p. Oxford, UK.

Bosenick, A., Geiger, C.A., Schaller, T., and Sebald, A. (1995) An ^{29}Si MAS NMR and IR spectroscopic investigation of synthetic pyrope-grossular garnet solid solutions. American Mineralogist. 80, 691-704.

Bosenick, A., Geiger, C.A., and Phillips, B. (1999) Local Ca-Mg distribution of Mg-rich pyrope-grossular garnets synthesized at different temperatures revealed by ^{29}Si NMR MAS spectroscopy. American Mineralogist. 42, 1422-1433.

Bosenick, A., Dove, M.T., and Geiger, C.A. (2000) Simulation studies of pyrope-grossular solid solutions. Physics and Chemistry of Minerals. 27, 398-418.

Burns, R.G. and Huggins, F.E. (1972) Cation determinative curves for Mg-Fe-Mn olivines from vibrational spectra. American Mineralogist. 57, 967-985.

Cococcioni, M., Dal Corso, A., and de Gironcoli, S. (2003) Structural, electronic, and magnetic

properties of Fe_2SiO_4 fayalite: Comparison of LDA and GGA results. Physical Review. B 67, 094106-1-094106-7.

Dachs, E. and Geiger, C.A. (2019) Thermodynamic behavior of grossular-andradite, $Ca_3(Al_xFe^{3+}_{1-x})_2Si_3O_{12}$, garnets: A calorimetric study. European Journal of Mineralogy. DOI: 10.1127/ejm/2019/0031-2827.

Dachs, E., Geiger, C.A., von Seckendorff, V. and Grodzicki, M. (2007) A low-temperature calorimetric study of synthetic forsterite-fayalite (Mg_2SiO_4-Fe_2SiO_4) solid solutions: An analysis of vibrational, magnetic and electronic contributions to the molar heat capacity and entropy of mixing. Journal of Chemical Thermodynamics. 39, 906-933.

Dachs, E., Geiger, C.A., Withers, A.C. and Essene, E.J. (2009) A calorimetric investigation of spessartine: Vibrational and magnetic heat capacity. Geochimica Cosmochimica Acta. 73, 3393-3409.

Dachs, E., Geiger, C.A. and Benisek, A. (2012) Almandine: Lattice and non-lattice heat capacity behavior and standard thermodynamic properties. American Mineralogist. 97, 1171-1182.

Dachs, E., Geiger, C.A. and Benisek, A. (2014a) Thermodynamic mixing properties and behavior of grossular-spessartine, $(Ca_xMn_{1-x})_3Al_2Si_3O_{12}$, solid solutions. Geochimica Cosmochimica Acta, 141, 294-302.

Dachs E., Geiger C.A., Benisek, A. and Grodzicki, M. (2014b) Thermodynamic mixing properties and behavior of almandine-spessartine solid solutions. Geochimica Cosmochimica Acta. 125, 210-224.

de Gennes, P.G. (1960) Effects of double exchange in magnetic crystals. Physical Review. 118, 141-154.

de Oliveira, J.C.P, da Costa, Jr., M.I., Schreiner, W.H., and Vasquez, V. (1991) Magnetic properties of some iron-poor natural olivines. Journal of Magnetism and Magnetic Materials. 98, 239-244.

588 Geiger, C.A. (2000) Volumes of mixing in aluminosilicate garnets: Implications for solid
589 solution behavior. American Mineralogist. 85, 893-897.
590 Geiger, C.A., ed. (2001) Oxide and Silicate Solid Solutions of Geological Importance.
591 European Mineralogical Union Notes in Mineralogy, v. 3, Eötvös University Press. 465
592 p.
593 Geiger, C.A. (2008) Silicate garnet: A micro to macroscopic (re)view. American
594 Mineralogist. 93, 360-372.
595 Geiger, C.A. (2013) Static disorders of atoms and experimental determination of Debye
596 temperature in pyrope: Low- and high-temperature single-crystal X-ray diffraction
597 study -- Discussion. American Mineralogist. 98, 780-782.
598 Geiger, C.A. (2013) Garnet: A key phase in nature, the laboratory and in technology.
599 Elements. 9, 447-452.
600 Geiger, C.A. and Rossman, G.R. (1994) Crystal field stabilization energies of almandine-
601 pyrope and almandine-spessartine garnets determined by FTIR near infrared
602 measurements. Physics and Chemistry of Minerals. 21, 516-525.
603 Geiger, C.A. and Feenstra, A. (1997) Molar volumes of mixing of almandine-pyrope and
604 almandine-spessartine garnets and the crystal chemistry of aluminosilicate garnets.
605 American Mineralogist. 82, 571-581.
606 Geiger, C.A., Langer, K., Winkler, B., and Cemic, L. (1988) The synthesis, characterisation and
607 physical properties of end-member garnets in the system $(Fe,Mg,Ca,Mn)_3Al_2(SiO_4)_3$. In
608 High Pressure Geosciences and Material Synthesis, Proceedings XXV. Annual Meeting
609 European High Pressure Research Group, Ed. Vollstädt, H., Akademie-Verlag Berlin,
610 193-198.
611 Geiger, C.A., Dachs, E., Vielreicher, N., and Rossman, G.R. (2018) Heat capacity behavior of
612 andradite: A multi-sample and -methodological investigation. European Journal of
613 Mineralogy, European Journal of Mineralogy. 30, 681-694.
614 Geller, S. (1967) Crystal chemistry of garnets. Zeitschrift für Kristallographie. 125, 1-47.

615 Goodenough, J.B. (1963) Magnetism and the Chemical Bond. 393 p. John Wiley and Sons.
616 New York.
617 Gopal, E.S.R. (1966) Specific heats at low temperatures. New York, Plenum Press. 240 p.
618 Grimvall, G. (1986) Thermophysical Properties of Materials. Elsevier Science Publications.
619 New York. 348 p.
620 Heinemann, R., Kroll, H., Kirfel, A., and Barbier, B. (2007) Order and anti-order in olivine
621 III: Variation of the cation distribution in the Fe,Mg olivine solid solution series with
622 temperature and composition. European Journal of Mineralogy. 19, 15-27.
623 Klemme, S., van Miltenburg, J. C., Javorsky, P., and Wastin, F. (2005) Thermodynamic
624 properties of uvarovite garnet $Ca_3Cr_2Si_3O_{12}$. American Mineralogist. 90, 663-665.
625 Komada, N. (1986) Measurement and interpretation of heat capacities of several inorganic
626 substances, Ph.D. Thesis, Department of Chemistry, University of Michigan, 384 p.
627 Komada, N. and Westrum, E.F. (1997) Modeling lattice heat capacity contributions by a
628 single-parametric phonon dispersion approach. Journal of Chemical Thermodynamics.
629 29, 311-336.
630 Kolesov, B.A. and Geiger, C.A. (2004) A temperature-dependent single-crystal Raman
631 spectroscopic study of fayalite: evidence for phonon-magnetic excitation coupling.
632 Physics and Chemistry of Minerals. 31, 155-161.
633 Lau, G.C., Klimczuk, T., Ronning, F., McQueen, T.M., and Cava, R.J. (2009) Magnetic
634 properties of the garnet and glass forms of $Mn_3Al_2Si_3O_{12}$. Physical Review B. 80,
635 21441(5).
636 Lottermoser, W., Müller, R., and Fuess, H. (1986) Antiferromagnetism in synthetic olivines.
637 Journal of Magnetism and Magnetic Materials. 54-57, 1005-1006.
638 McCarty, R.J., Palke, A.C., Stebbins, J.F., and Hartman, J.S. (2015) Transition metal cation site
639 preferences in forsterite (Mg_2SiO_4) determined from paramagnetically shifted NMR
640 resonances. American Mineralogist. 100, 1265-1276.

641 Menzer, G. (1928) Die Kristallstruktur der Granate. Zeitschrift für Kristallographie. 69, 300-
642 396.
643 Meyer, A., Pascale, F., Zicovich-Wilson, C.M, and Dovesi, R. (2010) Magnetic interactions
644 and electronic structure of uvarovite and andradite garnets. An ab-initio all-electron
645 simulation with the program Crystal06 program. International Journal of Quantum
646 Chemistry. 110, 338-351.
647 Mittal, R., Chaplot, S.L., Choudhury, N., and Loong, C.-K. (2000) Inelastic neutron
648 scattering and lattice-dynamics studies of almandine $Fe_3Al_2Si_3O_{12}$. Physical Review B,
649 61 (6), 3983-3988.
650 Müller, R., Feuss, H., and Brown, P.J. (1982) Magnetic properties of synthetic fayalite (α-
651 Fe_2SiO_4) Journal de Physique Colloques. 43, C7-249-252.
652 Murad, E. (1984) Magnetic ordering in andradite. American Mineralogist. 69, 722-724.
653 Murad, E. and Wagner, F.E. (1987) The Mössbauer spectrum of almandine. Physics and
654 Chemistry of Minerals. 14, 264-269.
655 Néel, M.L. (1948) Propriétés magnétiques des ferrites; ferrimagnétisme et
656 antiferromagnétisme. Annales de Physique. 12, 137-198.
657 Novak, G.A. and Gibbs, G.V. (1971) The crystal chemistry of the silicate garnets. American
658 Mineralogist. 56, 791-825.
659 Palke, A.C., Stebbins, J.F., Geiger, C.A., and Tippelt, G. (2015) Cation order-disorder in Fe-
660 bearing pyrope and grossular garnets: An ^{27}Al and ^{29}Si MAS NMR and ^{57}Fe Mössbauer
661 spectroscopy study. American Mineralogist. 100, 536-547.
662 Palke, A.C. and Geiger, C.A. (2016) Trivalent transition-metal cations and local structure in
663 synthetic pyrope- and grossular-rich solid solutions investigated by ^{27}Al and ^{29}Si MAS
664 NMR spectroscopy. European Journal of Mineralogy. 28, 179-187.

665 Panissod, P. and Drillon M. (2003) Magnetic ordering due to dipolar interaction in low
666 dimensional materials. In J.S. Miller and M. Drillon, Eds., p. 233-270. Magnetism:
667 Molecules to Materials IV. Wiley-VCH. Berlin, BRD.
668 Parks, G.A. and Akhtar, S. (1968) Magnetic moment of Fe^{2+} in paramagnetic minerals. The
669 American Mineralogist. 53, 406-415.
670 Pilati, T., Demartin, F., and Gramaccioli, C.M. (1996) Atomic displacement parameters for
671 garnets: A lattice-dynamical evaluation. Acta Crystallographica. B52, 239-250.
672 Plakhty, V., Golosovsky, I., Gukasov, A., Smirnov, O., Brückel, T., Dorner, B., and Burlet,
673 P. (1993) Spin waves and exchange interactions in the antiferromagnetic garnets with
674 Fe^{3+} in the octahedral sites. Zeitschrift für Physik. B92, 443-449.
675 Prandl, W. (1971) Die magnetische Struktur und die Atomparameter des Almandins
676 $Al_2Fe_3(SiO_4)_3$. Zeitschrift für Kristallographie. 134, 333-343.
677 Prandl, W. (1973) Rhombohedral magnetic structure of spessartine type garnets. Physica
678 Status Solidi. b. 55, K159-163.
679 Quartieri, S., Artioli, G., Deriu, A., Lottici, P.P. and Antonioli, G. (1993) ^{57}Fe-Mössbauer
680 investigation on garnets from the Ivrea-Verbano zone. Mineralogical Magazine. 57,
681 671-676.
682 Robie, R.A., Finch, C.B., and Hemingway, B.S. (1982) Heat capacity and entropy of fayalite
683 (Fe_2SiO_4) between 5.1 and 383 K: comparison of calorimetric and equilibrium values
684 for the QFM buffer reaction. American Mineralogist. 67, 463-469.
685 Rodehorst U., Carpenter, M.A., Boffa Ballaran, T. and Geiger, C.A. (2004) Local structural
686 heterogeneity, mixing behaviour and saturation effects in the grossular-spessartine solid
687 solution. Physics and Chemistry of Minerals. 31, 387-404
688 Santoro, R.P., Newnham, R.E., and Nomura, S. (1966) Magnetic properties of Mn_2SiO_4 and
689 Fe_2SiO_4. Journal of Physical and Chemistry of Solids. 27, 655-666.
690 Schmidt, W., Brotzeller, C., Geick, R., Schweiss, P., and Treutmann, W. (1992) Magnon-
691 phonon coupling in Fe_2SiO_4. Journal of Magnetism and Magnetic Materials. 104-107,

1049-1050.

Stebbins, J.F., McCarty, R.J., and Palke, A.C. (2018) Toward the wider application of ^{29}Si NMR spectroscopy to paramagnetic transition metal silicate minerals and glasses: Fe(II), Co(II) and Ni(II) silicates. American Mineralogist. 103, 776-791.

Stout, J.W. (1961) Magnetic transitions at low temperatures. Pure and Applied Chemistry. Issue 1-2, 287-296.

von Seckendorff, V. and O'Neill, H.St.C. (1993) Contributions to Mineralogy and Petrology. 113(2), 196-207.

Wijbrans, C.H., Neihaus, O., Rohrbach, A., Pöttgen, R., and Klemme, S. (2014) Thermodynamic and magnetic properties of knorringite garnet ($Mg_3Cr_2Si_3O_{12}$) based on low-temperature calorimetry and magnetic susceptibility measurements. Physics and Chemistry of Minerals. 41, 341-346.

Winkler, G. (1981) Magnetic Garnets. 735 p., vol. 5. Vieweg und Sohn, Braunschweig/Wiesbaden, BRD.

Woodland, A.B. and O'Neill, H.St.C. (1993) Synthesis and stability of $Fe_3^{2+}Al_2^{3+}Si_3O_{12}$ garnet and phase relations with $Fe_3Al_2Si_3O_{12}$-$Fe_3^{2+}Fe_2^{3+}Si_3O_{12}$ solutions. American Mineralogist. 78, 1000-1013.

Woodland, A.B., Droop, G., and O'Neill, H. St. C. (1995) Almandine-rich garnet from Collobrières, southern France, and its petrological significance. European Journal of Mineralogy. 7, 187-194.

Zener, C. (1951) Interaction between the *d*-shells in the transition metals. II. Ferromagnetic compounds of manganese with perovskite structure. Physical Review. 82, 403-40.

Zhrebetskyy, D., Lebernegg, S., Amthauer, G., and Grodzicki, M. (2012) Magnetic structure of almandine. Physics and Chemistry of Minerals. 39, 351-361.

This is a preprint, the final version is subject to change, of the American Mineralogist (MSA)
Cite as Authors (Year) Title. American Mineralogist, in press.
DOI: https://doi.org/10.2138/am-2019-6839CCBYNCND

Table 1. Neel temperature, T_N, for synthetic olivine and three garnet binary solid solutions as determined by relaxation calorimetry and magnetic susceptibility measurements.

Olivine	T_N[¥]	T_N[Ω]		Garnet*	T_N		Garnet[#]	T_N		Garnet[§,¶]	T_N
Fa_{100}	64.5(1)	67		Alm_{100}	9.2		Gro_{100}	-		Gro_{100}	-
$Fa_{90}Fo_{10}$	57.3(1)	59		$Alm_{75}Sps_{25}$	5.8		$Gro_{90}Sps_{10}$	< 2		$Gro_{75}And_{25}$	3.0
$Fa_{80}Fo_{20}$	49.5(1)	55		$Alm_{50}Sps_{50}$	4.2		$Gro_{75}Sps_{25}$	< 2		$Gro_{50}And_{50}$	4.4
$Fa_{70}Fo_{30}$	41.7(1)	45		$Alm_{25}Sps_{75}$	4.5		$Gro_{60}Sps_{40}$	< 2		$Gro_{25}And_{75}$	7.9
$Fa_{60}Fo_{40}$	32.8(1)	33		$Spessartine_{100}$	6.2		$Gro_{50}Sps_{50}$	2.3		$Andradite_{100}$	11.5
$Fa_{50}Fo_{50}$	29.8	21					$Gro_{40}Sps_{60}$	2.9			
$Fa_{40}Fo_{60}$	26.0	20					$Gro_{25}Sps_{75}$	4.1			
$Fa_{30}Fo_{70}$	25.3	-		[‡,∞]$Alm_{71}Sps_{26}$	6.7		$Gro_{20}Sps_{80}$	4.6		[‡,†]$Gro_{82}And_{13}$	2.5
$Fa_{20}Fo_{80}$	-	-		[‡,∞]$Alm_{36}Sps_{62}$	3.5		$Gro_{15}Sps_{85}$	5.0		[‡,†]$Gro_{74}And_{19}$	3.0
$Fa_{10}Fo_{90}$	18.6	-					$Gro_{10}Sps_{90}$	5.4		[‡,†]$Gro_{73}And_{23}$	3.0
$Forsterite_{100}$	-	-					$Spessartine_{100}$	6.2			

T_N values synthetic olivine: [¥]Dachs et al. (2007) and [Ω]Belley et al. (2009). T_N values: synthetic and [‡] natural (extra minor elements not considered) garnet: *Dachs et al. (2012a; 2014b), [#]Dachs et al. (2014a), [§]Geiger et al. (2018) and [¶]Dachs and Geiger (2019). Compositions in [∞]Geiger and Rossman (1994) and [†]Dachs and Geiger (2019).

Figures

Figure 1. Néel temperature, T_N, behavior for fayalite-forsterite, $Fe^{2+}_2SiO_4$-Mg_2SiO_4, olivines. The solid black points give T_N for each olivine composition (errors in T_N are discussed in the text). The data can be described by two linear segments (black dashed lines) or a third-order order polynomial (solid black line). The blue dashed line connects Fa_{100} and $Fa_{10}Fo_{90}$. At the bottom of the figure, values for the excess magnetic entropy of mixing for different composition olivines are given by the red diamonds (Dachs et al. 2007). The solid red line represents a 3rd-order polynomial fit to the data. The dashed red line represents ideal magnetic entropy of mixing behavior.

Supplementary Figure la (Appendix I). T_N behavior for $Fe^{2+}_2SiO_4$-Mg_2SiO_4 olivines given by low-temperature C_p and magnetic susceptibility measurements. Black circles: Dachs et al. (2007) and red circles: Belley et al. (2009).

Figure 2. Néel temperature, T_N, behavior for three garnet binary substitutional solid solutions. a.) grossular-andradite - $Ca_3(Al_x,Fe^{3+}_{1-x})_2Si_3O_{12}$, b.) grossular-spessartine - $(Ca_x,Mn^{2+}_{1-x})_3Al_2Si_3O_{12}$, and c.) almandine-spessartine - $(Fe^{2+}_x,Mn^{2+}_{1-x})_3Al_2Si_3O_{12}$. The two dashed lines show linear-segment fits to the respective data. The solid curves represent third-order polynomial fits.

Fig. 3. a.) Polyhedral model of fayalite, Fe_2SiO_4. The isolated SiO_4 tetrahedra are shown in red. The M1 (light brown) and M2 (dark brown) sites contain Fe^{2+} in octahedral coordination. b.) M1 octahedra, forming infinite chains, showing the common O1 (dark green colored "beachballs") and O2 (middle green colored "beachballs") anions constituting a shared octahedral edge. c.) M2 octahedra showing corner-sharing O2 oxygens (middle green colored "beachballs") and unshared O1 (solid middle green spheres) and O3 (solid bright green spheres) oxygens. d.) M1 and M2 octahedral showing common edge-shared O3 (bright green colored "beachballs") and O2 oxygens (middle green colored "beachballs").

Figure 4. a.) Polyhedral model of silicate garnet. The SiO_4 tetrahedra and AlO_6 octahedra share corners, building a quasi-three-dimensional framework. The *X* cations (yellow spheres) are located in small cavities of triangular dodecahedron coordination. b.) In andradite two $Fe^{3+}O_6$ octahedra with Fe^{3+} given by the medium-colored green spheres and a central SiO_4 tetrahedron (Si cation dark green). One local superexchange bridge is given by the green colored cations

(Meyer et al. 2010) and the oxygen anions by "beachball" spheres via Fe^{3+}-O-(Si)-O-Fe^{3+}. c.) A second possible superexchange in andradite is given by Fe^{3+}-O-(Ca - light green)-O-Fe^{3+} bridges (Meyer et al. 2010). d.) One possible relationship between neighboring edge-sharing XO_8 groups for a given almandine-spessartine solid solution (Fe^{2+} - dark brown and Mn^{2+} - light brown). "Normal" ferromagnetic superexchange occurs through oxygen anions Zhrebetskyy et al. (2012). Double exchange occurs through the "beachball"-illustrated oxygens. Note that the relative sizes of the various ions are not correct, but made to make the local magnetic interactions easier to visualize.

Figure 5. $C_p(T)_{mag}$ behavior for almandine (red), spessartine (green) and andradite (blue) normalized to one transition-metal-cation. The three λ-peaks were obtained through calorimetric measurements (Dachs et al. 2012; Dachs et al. 2009; Geiger et al. 2018). T_N is measurable to better than ± 0.2 K. Note the λ-peak for andradite and the presence of a weak shoulder on the low-temperature flank. Its origin is discussed in the text.

This is a preprint, the final version is subject to change, of the American Mineralogist (MSA)
Cite as Authors (Year) Title. American Mineralogist, in press.
DOI: https://doi.org/10.2138/am-2019-6839CCBYNCND

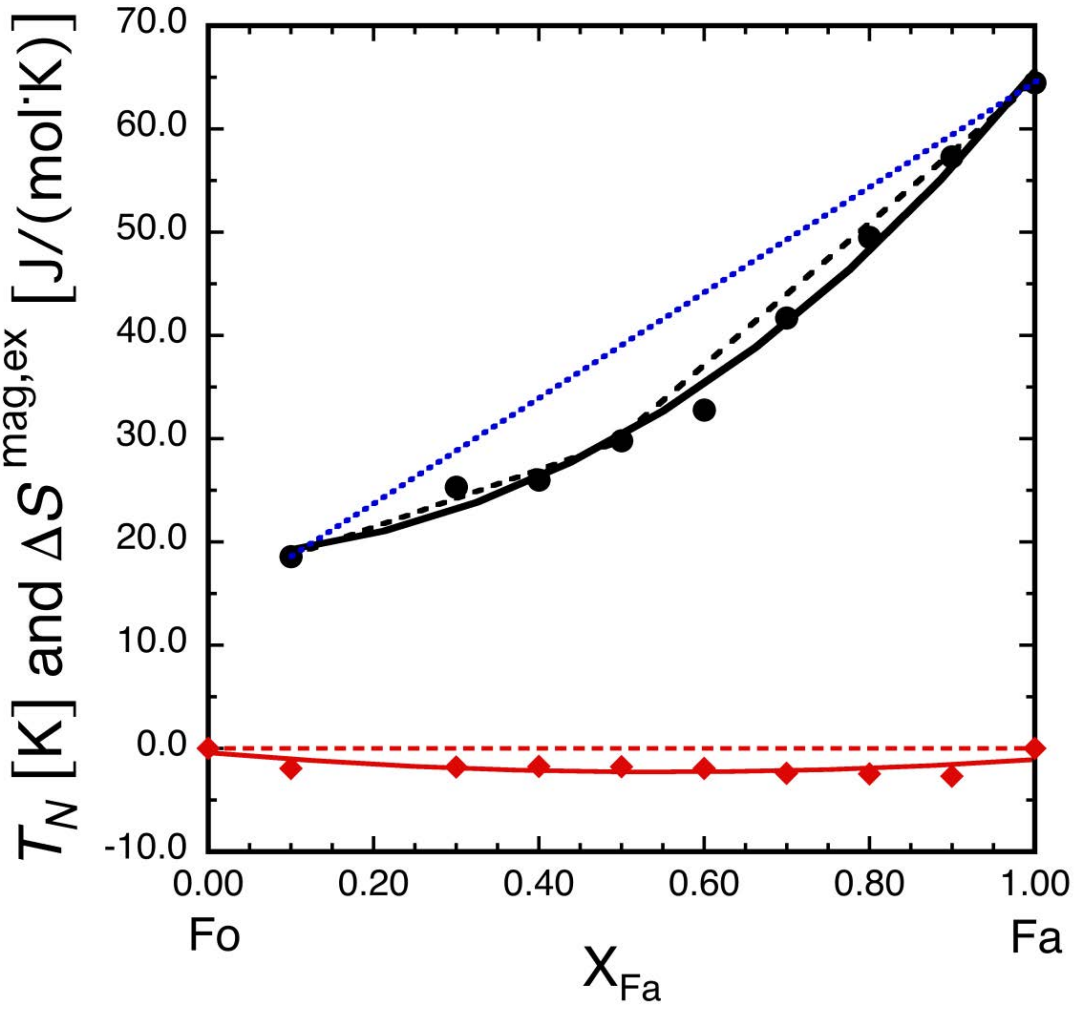

Figure 1.

This is a preprint, the final version is subject to change, of the American Mineralogist (MSA)
Cite as Authors (Year) Title. American Mineralogist, in press.
DOI: https://doi.org/10.2138/am-2019-6839CCBYNCND

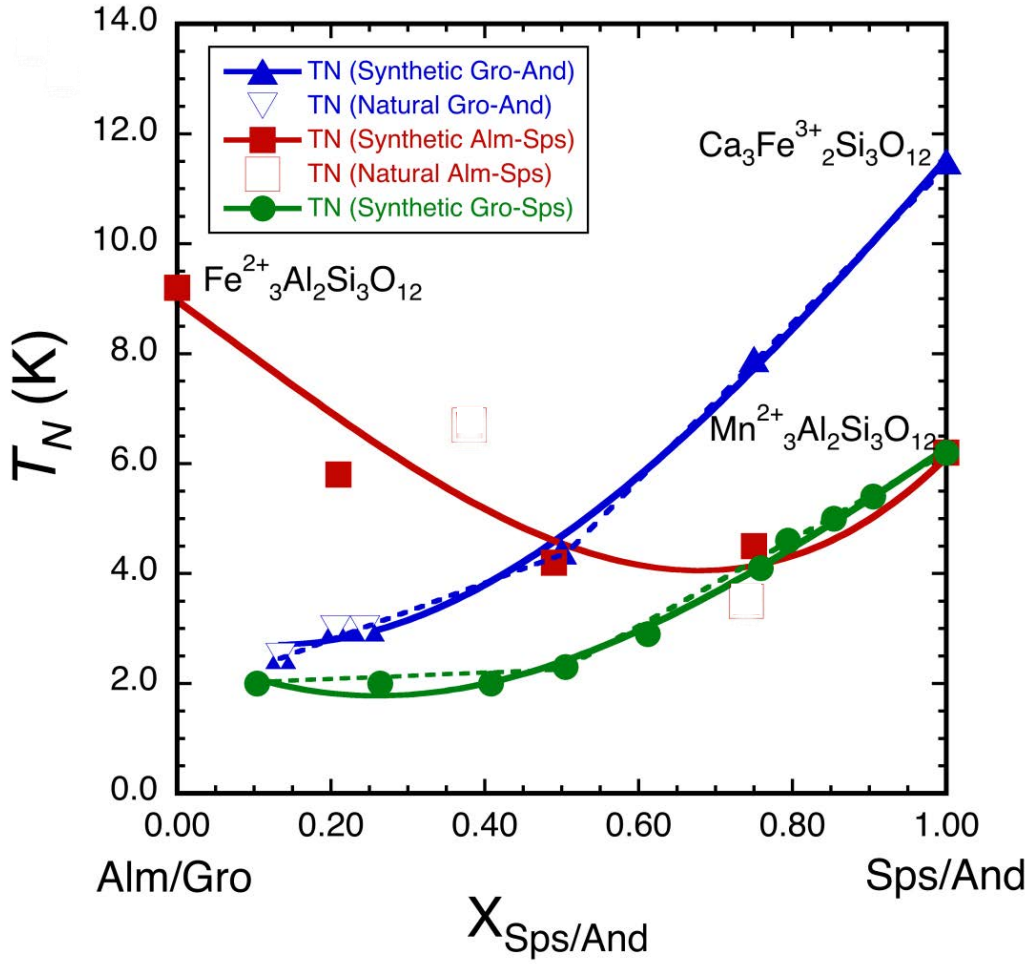

Figure 2.

This is a preprint, the final version is subject to change, of the American Mineralogist (MSA)
Cite as Authors (Year) Title. American Mineralogist, in press.
DOI: https://doi.org/10.2138/am-2019-6839CCBYNCND

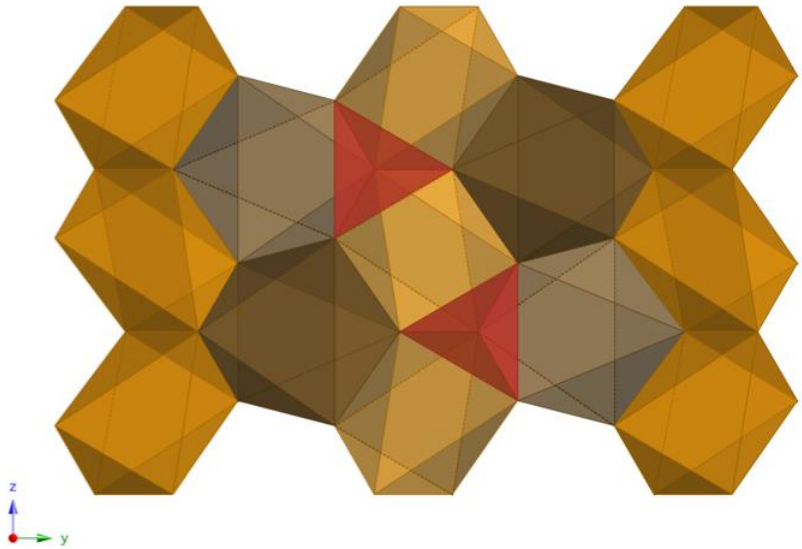

a.)

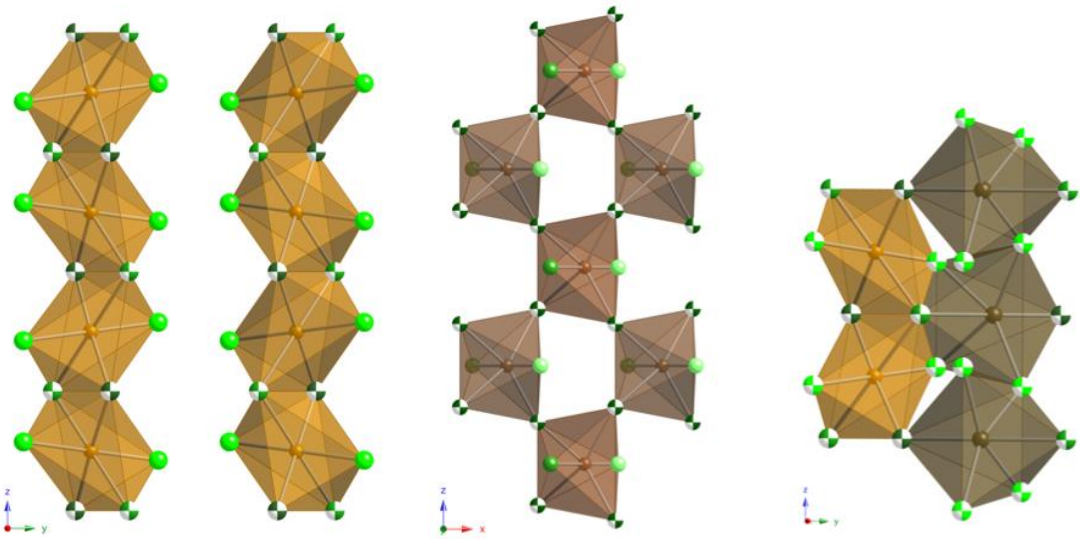

b.) c.) d.)

Figure 3a, b, c and d.

This is a preprint, the final version is subject to change, of the American Mineralogist (MSA)
Cite as Authors (Year) Title. American Mineralogist, in press.
DOI: https://doi.org/10.2138/am-2019-6839CCBYNCND

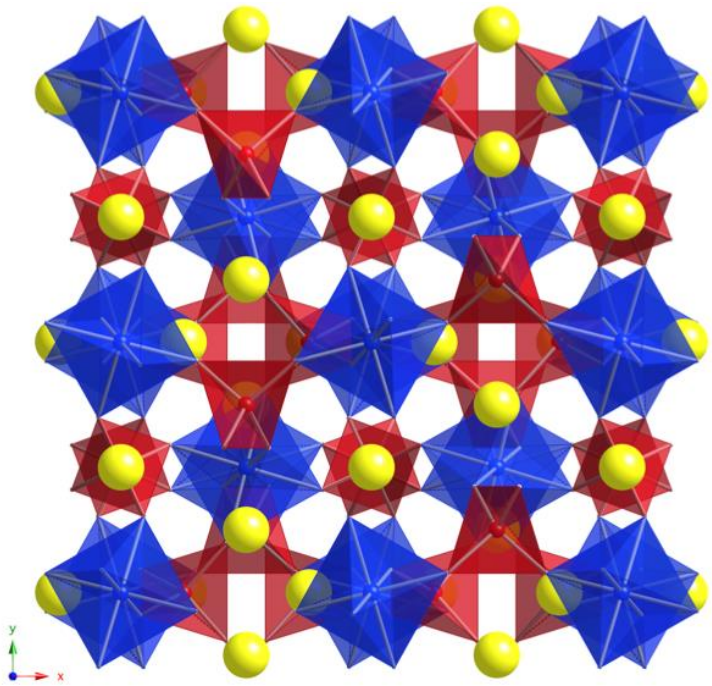

a.)

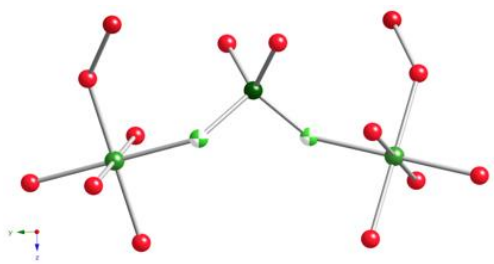

b.)

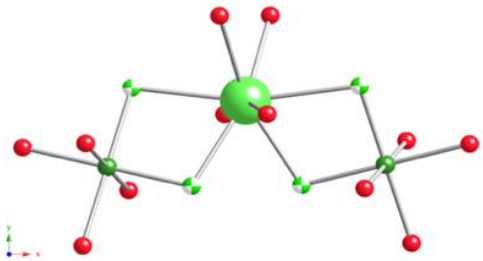

c.)

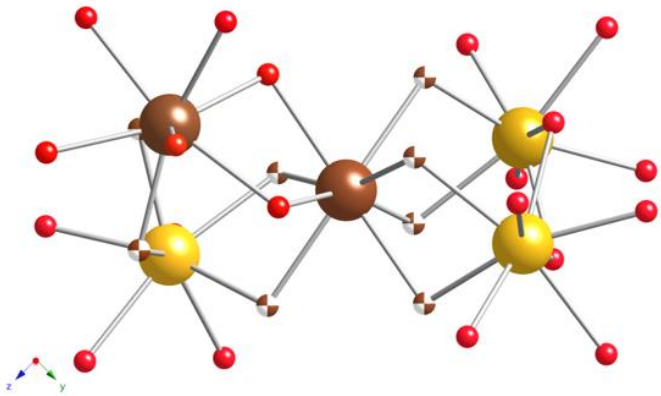

d.)

Figure 4a, b, c, and d.

This is a preprint, the final version is subject to change, of the American Mineralogist (MSA)
Cite as Authors (Year) Title. American Mineralogist, in press.
DOI: https://doi.org/10.2138/am-2019-6839CCBYNCND

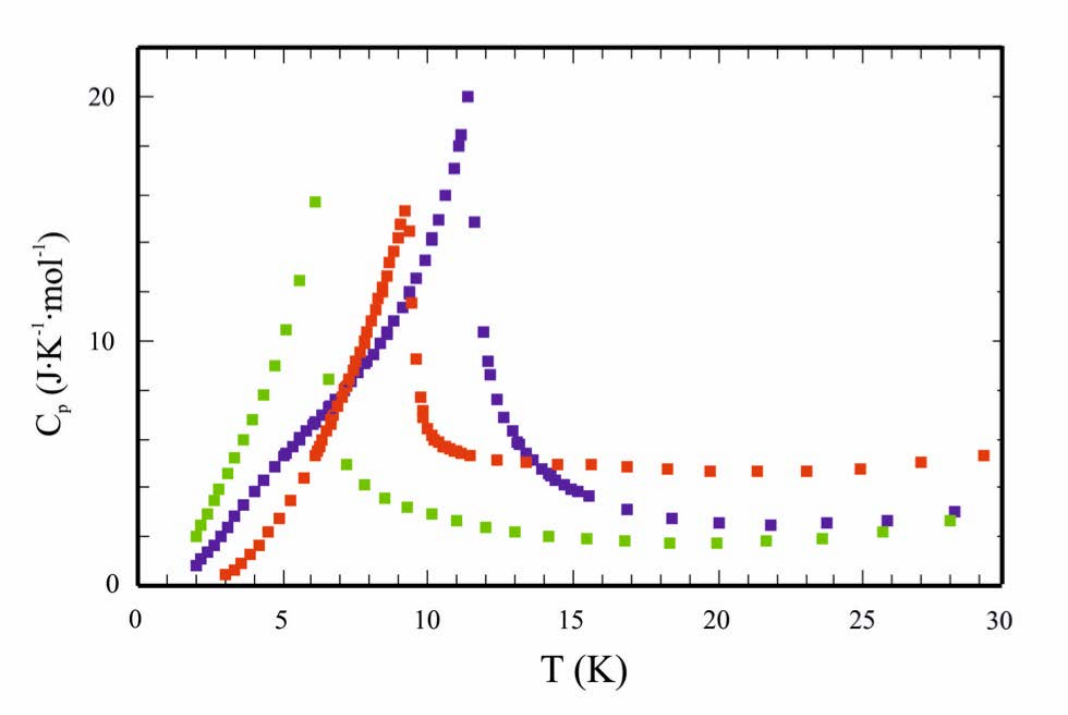

Figure 5.

This is a preprint, the final version is subject to change, of the American Mineralogist (MSA)
Cite as Authors (Year) Title. American Mineralogist, in press.
DOI: https://doi.org/10.2138/am-2019-6839CCBYNCND

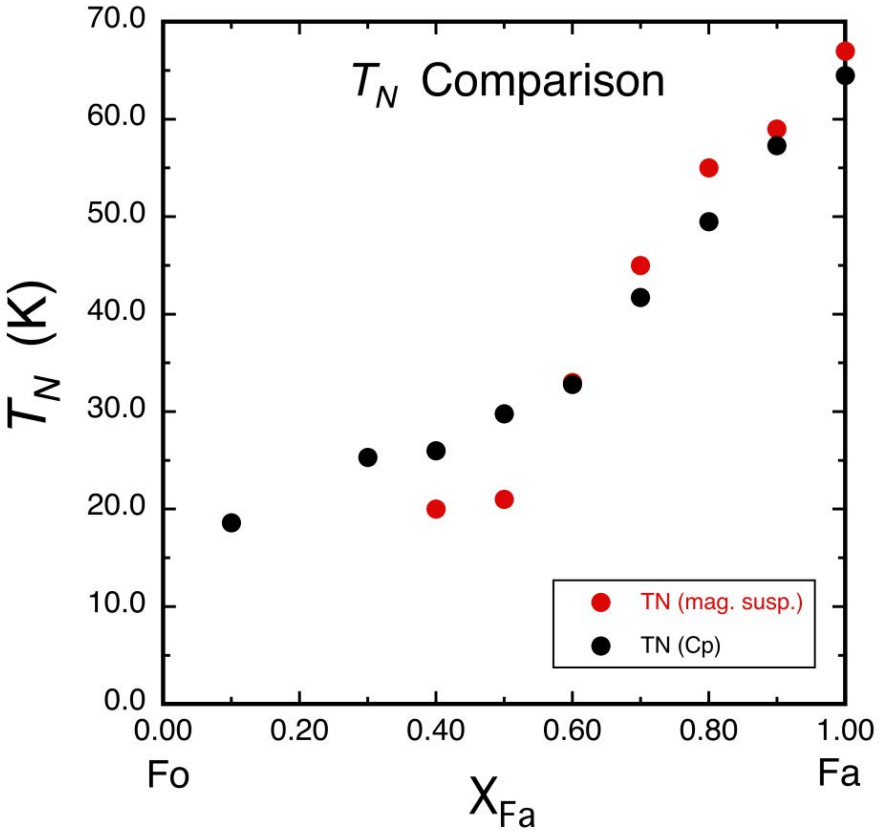

Supplementry Figure 1a.